Journal of Power Sources 215 (2012) 258–265

Contents lists available at SciVerse ScienceDirect

Journal of Power Sources

journal homepage: www.elsevier.com/locate/jpowsour

Improving the high rate performance of $Li_4Ti_5O_{12}$ through divalent zinc substitution

Ting-Feng Yi [a,*], Haiping Liu [b,**], Yan-Rong Zhu [a], Li-Juan Jiang [a], Ying Xie [c,***], Rong-Sun Zhu [a]

[a] School of Chemistry and Chemical Engineering, Anhui University of Technology, Maanshan, Anhui 243002, PR China
[b] School of Marine Science and Technology, Harbin Institute of Technology, Weihai, Shandong 264209, PR China
[c] Key Laboratory of Functional Inorganic Material Chemistry, Ministry of Education, Heilongjiang University, Harbin 150080, PR China

HIGHLIGHTS

- The over-discharge performance $Li_4Ti_{5-x}Zn_xO_{12}$ ($0 \le x \le 0.2$) anode is first reported.
- Zn doping improves the conductivity and reversibility of the $Li_4Ti_5O_{12}$.
- $Li_4Ti_{4.8}Zn_{0.2}O_{12}$ anode remarkably exhibits high rate performance.

GRAPHICAL ABSTRACT

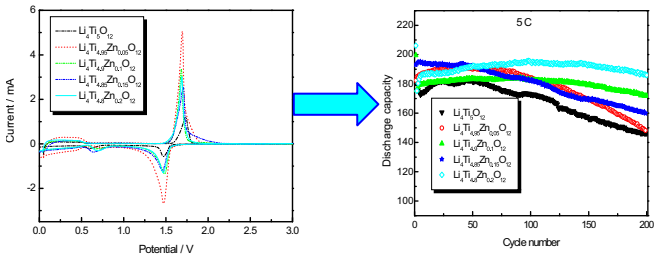

ARTICLE INFO

Article history:
Received 14 January 2012
Received in revised form
27 March 2012
Accepted 26 April 2012
Available online 22 May 2012

Keywords:
Lithium-ion battery
Anode
Spinel lithium titanium oxide
Zinc doping
Rate performance

ABSTRACT

Microscale $Li_4Ti_{5-x}Zn_xO_{12}$ ($0 \le x \le 0.2$) particles with high phase purity were synthesized by a simple solid-state reaction. The effect of the zinc doping on the physicochemical properties of $Li_4Ti_5O_{12}$ (LTO) was extensively studied by TG-DSC, XRD, Raman spectroscopy, SEM, CV, EIS, and galvanostatic charge–discharge testing. The crystallization of lithium titanate oxide forms at about 750 °C. The lattice parameter of the Zn-doped LTO samples is slightly smaller than that for the pure LTO samples, and zinc doping does not change the basic $Li_4Ti_5O_{12}$ structure. Even though the material has a particle size of 1–2 μm, Zn-doped LTO shows very high excellent capacity retention between 0 and 2.5 V. Especially, in rate performance, the $Li_4Ti_{4.8}Zn_{0.2}O_{12}$ sample maintains capacity of about 180 mAh g^{-1} until 5 C rates after 200 cycles, while the pure LTO sample shows severe capacity decline at corresponding rates. The reason for the high rate performance of Zn-doped LTO anode is ascertained to the diffusion coefficient (D_{Li}) and reversible intercalation and deintercalation of lithium ion. The superior cycling performance and wide discharge voltage range, as well as simple synthesis route and low synthesis cost of the Zn-doped LTO are expected to show a potential commercial application.

1. Introduction

New generation lithium-ion batteries have been considered as the important power source for EV, HEV and PHEV due to the properties in terms of lightness, compactness, working voltage and energy density. However, the large use of lithium-ion batteries for low emission vehicles is presently slowed down by a series of issues, the most critical of them being concerns about safety [1]. One of the key safety issues would be the dendritic lithium growth on the anode surface at high charging current because

* Corresponding author. Tel.: +86 555 2311807; fax: +86 555 2311552.
** Corresponding author.
*** Corresponding author.
E-mail addresses: tfyihit@163.com (T.-F. Yi), hpliuhit@126.com (H. Liu), xieying@hlju.edu.cn (Y. Xie).

0378-7753/$ – see front matter © 2012 Elsevier B.V. All rights reserved.
doi:10.1016/j.jpowsour.2012.04.080

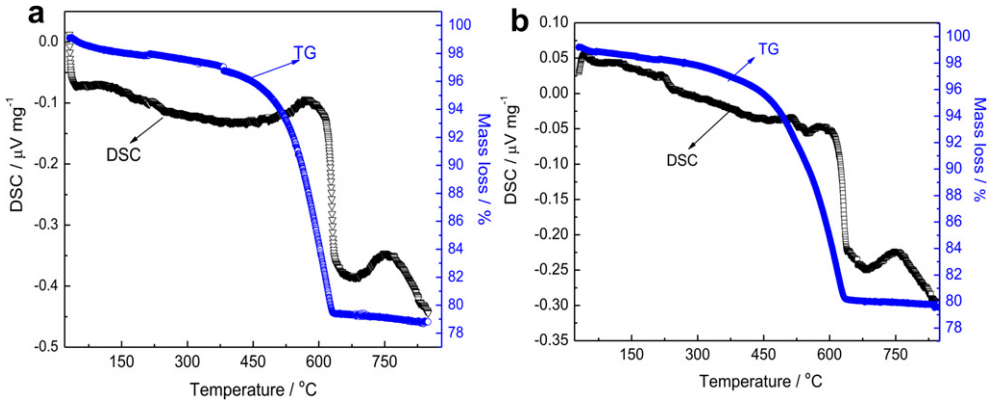

Fig. 1. TG/DSC curves of the mixture of precursor powders: (a) $Li_4Ti_5O_{12}$; (b) $Li_4Ti_{4.95}Zn_{0.05}O_{12}$.

the conventional carbonous materials approach almost 0 V versus Li^+/Li at the end of Li insertion [2]. Developing anode materials with high safety is one of the key challenges for lithium-ion batteries. $Li_4Ti_5O_{12}$ (LTO) has been investigated as a powerful anode material, because of its mid-discharge voltage close to 1.55 V versus Li^+/Li and high structural stability (zero-strain insertion material) in the charge–discharge process [3–8]. Unfortunately, the electrochemical properties of LTO might not be sufficient for high current applications before any materials modifications due to the poor electronic and lithium-ionic conductivities [9]. As a result several methods have been used to increase electronic conductivity with the intent of improving rate capability. These include forming a composite of $Li_4Ti_5O_{12}$ and a conductive second phase, doping $Li_4Ti_5O_{12}$ with Zn^{2+} [10], Mg^{2+}, Ni^{3+}, Al^{3+}, Cr^{3+}, Co^{3+}, Fe^{3+}, Mn^{3+}, Ga^{3+}, Zr^{4+}, Mo^{4+}, V^{5+}, Ta^{5+}, Nb^{5+} [11,12], F^- and Br^- in Li, Ti or O site [13]. In addition, the higher working potential of LTO compared with other anodes also limits the application LTO for high energy density devices because energy density is basically defined as the product of capacity and working potential. In addition, it is important to study the over-discharge behaviors of negative electrode materials at lower voltage considering the safety resulting from short circuit or abuse of anode material. There is not much report to operate LTO at a lower working potential less than 1 V. Our groups' report [12,14] suggests that this spinel anode has a relatively higher discharge capacity, because it displays reversible capacity in the lower operating voltage range (0–2 V) than that previously contemplated. It is well known that the zinc is abundant and less expensive than the many transition metals, so Zn-substituted $Li_4Ti_5O_{12}$ spinel is expected to be an anode material with lower cost than other transition metals substituted $Li_4Ti_5O_{12}$. Zhang et al. [10] reported the doping with Zn^{2+} in the form of $Li_{4-x}Zn_xTi_5O_{12}$ ($x = 0, 0.25, 0.5, 1$), and rate capability of LTO cycled between 1 and 2.5 V is improved. To our knowledge, no investigation was reported on the electrochemical characteristics of Zn-doped LTO ($Li_4Ti_{5-x}Zn_xO_{12}$) in the Ti site discharged to 0 V. Although LTO can be synthesized by sol–gel method [15], composite molten-salt method (CMSM) [16] and modified rheological phase reaction [17], etc., they have some other disadvantages, such as complicated synthetic routes and high synthetic cost, which is difficult for commercial applications. From a commercial viewpoint, the solid-state synthesis of LTO powders exhibits a potential commercial application due to the simple synthesis route and low synthesis cost. In the present work we report on the study performed on Zn-doped $Li_4Ti_5O_{12}$ compound in the Ti site prepared by a solid-state method. A careful investigation has been carried out to give new insights into the structural properties, the rate performance, over-discharge performance (discharged to 0 V), and the doping effect on the conductivity of the material.

2. Experimental

The Zn-doped powder samples were prepared by treating in air at 1123 K for 24 h a mixture of TiO_2, Li_2CO_3, and $Zn(NO_3)_2 \cdot 6H_2O$ in proper amount, to form $Li_4Ti_{5-x}Zn_xO_{12}$ ($x = 0, 0.05, 0.1, 0.15, 0.2$).

The electrodes for electrochemical testing were prepared by pasting a slurry containing 80 wt% $Li_4Ti_{5-x}Zn_xO_{12}$, 10 wt% carbon black and 10 wt% polyvinylidene fluoride (PVDF) dissolved in N-methylpyrolline onto a copper foil with the doctor blade

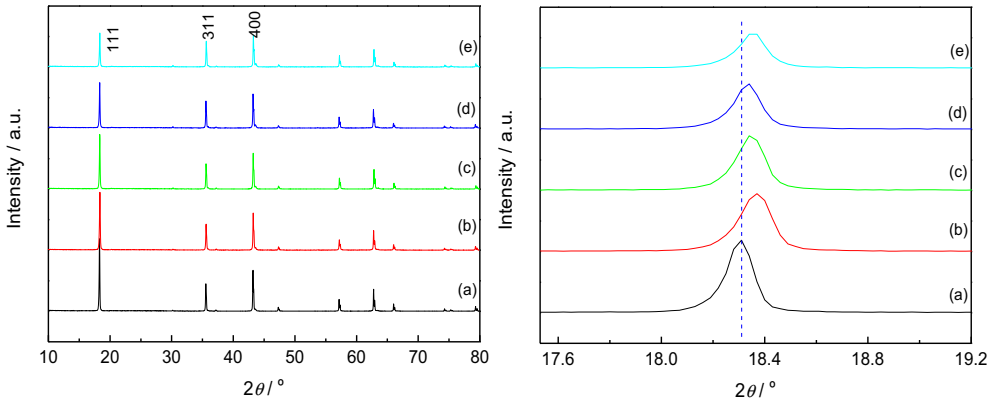

Fig. 2. XRD pattern of as-prepared $Li_4Ti_{5-x}Zn_xO_{12}$: (a) $x = 0$; (b) $x = 0.05$; (c) $x = 0.1$; (d) $x = 0.15$; (e) $x = 0.2$.

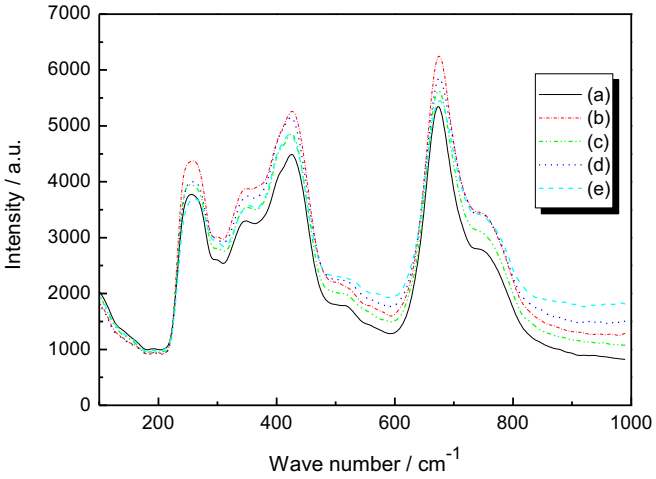

Fig. 3. Raman spectra of $Li_4Ti_{5-x}Zn_xO_{12}$: (a) $x = 0$; (b) $x = 0.05$; (c) $x = 0.1$; (d) $x = 0.15$; (e) $x = 0.2$.

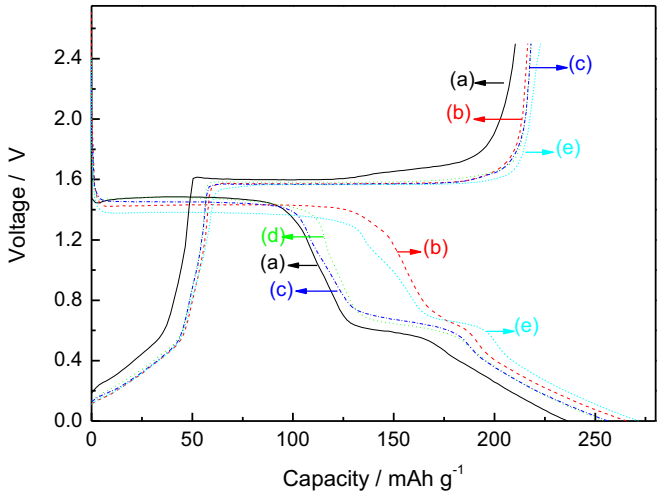

Fig. 5. Initial charge–discharge characteristics curves of $Li_4Ti_{5-x}Zn_xO_{12}$/Li coin cells carried out galvanostatically between 0 and 2.5 V at 0.5 C charge–discharge rate: (a) $x = 0$, (b) $x = 0.05$, (c) $x = 0.1$, (d) $x = 0.15$ and (e) $x = 0.2$.

technology. After coating, the film was dried in a vacuum oven at 100 °C for 12 h, pressed, and then cut into a sheet. The thickness of electrode prepared in this study is about 30 μm. Before using, the sheet was dried in a vacuum chamber at 120 °C for 10 h. Two-electrode batteries (CR2032) for cycles were assembled in an Ar-filled glove box using a metal lithium foil as counter electrode, 1 M $LiPF_6$ in a 1:1 (v/v) mixture of ethylene carbonate (EC) and dimethyl carbonate (DMC) as electrolyte and Celgard 2300 polypropylene as separator.

TG/DSC measurements were conducted on NETZSCH STA 449C differential scanning calorimeter at a scanning rate of 5 °C min^{-1} from 30 to 830 °C in an air atmosphere. XRD was performed on Rigaku D/MAX-2400 X-ray diffractometer with Cu $K\alpha_1$ ($10° < 2\theta < 80°$) monochromated radiation in order to identify the crystalline phase. Raman measurements were performed on an SPEX-1403 Raman spectrometer. The laser light source was the 488 nm line of an Ar^+ laser excited at 400 mW. All the powder samples were pressed into pellets before measurements. The particle morphologies were examined with a scanning electron microscope (Hitachi, S-4000). Cyclic voltammograms of both electrodes were measured on an electrochemical workstation (CHI 852C) between 0 and 3 V (versus Li/Li^+). EIS measurements were carried out in two-electrode cells by using Zahner Zennium IM6ex electrochemical workstation with a ±5 mV ac signal and a frequency range from 10^4 to 0.01 Hz. The difference between two-electrode system and three-electrode system is that the impedance spectrum of the two-electrode system is equal to the sum of the spectra of the positive and the negative electrodes in a three-electrode system [18,19]. EIS measurement of fresh $Li_4Ti_{5-x}Zn_xO_{12}$ ($x = 0$, 0.05, 0.1)/Li batteries was performed at the potential of open circuit voltage (about 3.0 V). Charge–discharge performance was characterized galvanostatically on Land 2000 T (Wuhan, China) tester at 0.5 C, 3 C and 5 C charge–discharge rate between 0.0 and 2.5 V (versus Li^+/Li), respectively.

3. Results and discussion

Fig. 1 shows the TG–DSC curves of the mixture of precursor powders with a heating rate of 5 °C min^{-1} from room temperature to 830 °C in air. It can be seen that the little weight loss of the first region may be attributed to the superficial water loss due to the hygroscopic nature of the precursor complex. The DSC curve shows an endothermic peak at about 200 °C, which is attributed to the loss of water of chemical bond water in the samples. There are two broad exothermic peaks on the DSC curves, associating with a noticeable weight lose in the TG curve between 350 and 750 °C. The weight loss occurred during this stage because of a violent oxidation–decomposition reaction. It is due to the decomposition of the inorganic constituents of the precursor followed by crystallization of $Li_4Ti_{5-x}Zn_xO_{12}$ phase. When the temperature is above 750 °C, the TG curve is stationary, which indicates that the decomposition is almost complete. It can be concluded that the crystallization of lithium titanate has almost formed at about 750 °C, and that any further heating only makes the structure of samples more crystalline.

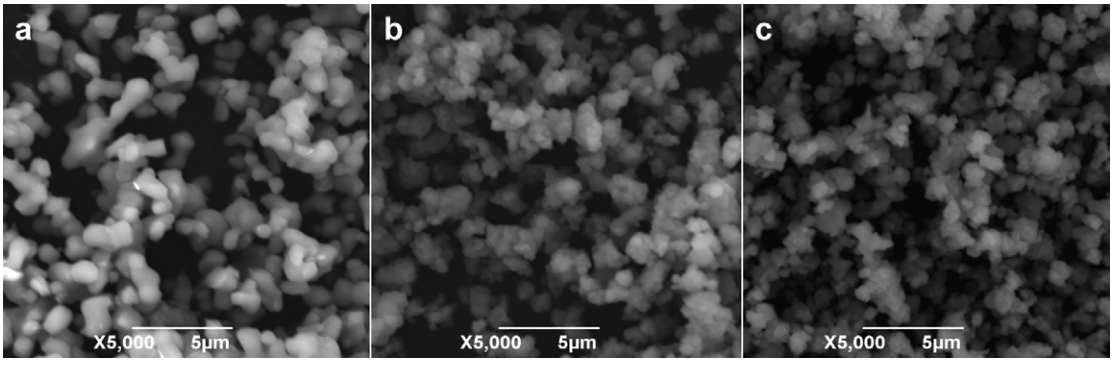

Fig. 4. SEM of the as-prepared $Li_4Ti_{5-x}Zn_xO_{12}$: (a) $x = 0$; (b) $x = 0.05$; (c) $x = 0.1$.

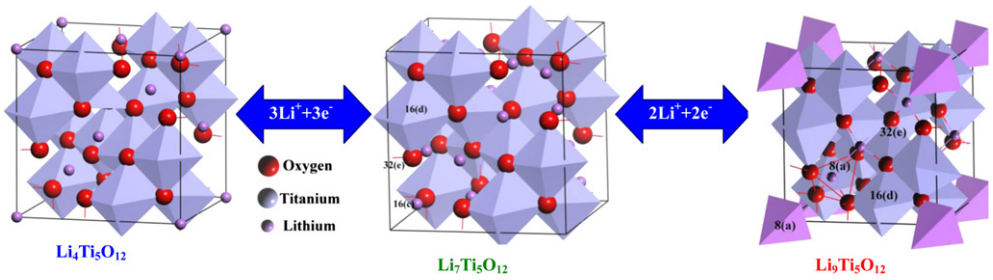

Fig. 6. Structure of $Li_4Ti_5O_{12}$, $Li_7Ti_5O_{12}$ and $Li_9Ti_5O_{12}$.

Based on the above analysis, it is necessary to calcine the precursor above 750 °C.

The XRD pattern of the annealed $Li_4Ti_{5-x}Zn_xO_{12}$ is shown in Fig. 2. All peaks were in accordance with the standard diffraction peaks of $Li_4Ti_5O_{12}$ with PDF number of 72-0426. This means that the low dose doping of Zn^{2+} cannot appear to change the basic $Li_4Ti_5O_{12}$ structure, but slightly changes the diffraction angle due to the atom size effect as plotted in Fig. 2. It can be found a slight shift

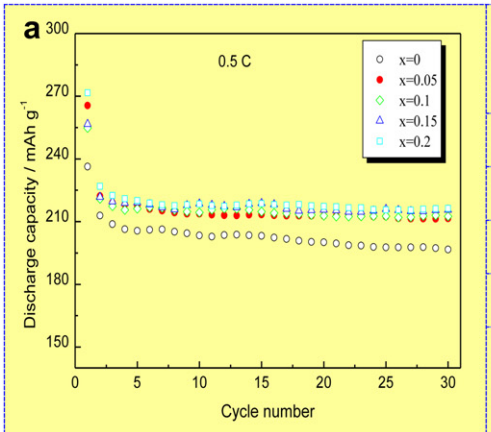

0.5 C charge-discharge rate	Initial capacity / mAh g^{-1}	Capacity after 30 cycles / mAh g^{-1}
$Li_4Ti_5O_{12}$	236.3	196.7
$Li_4Ti_{4.95}Zn_{0.05}O_{12}$	265.6	211.5
$Li_4Ti_{4.9}Zn_{0.1}O_{12}$	254.8	212.5
$Li_4Ti_{4.85}Zn_{0.15}O_{12}$	256.7	215.6
$Li_4Ti_{4.8}Zn_{0.2}O_{12}$	271.6	216.4

3 C charge-discharge rate	Initial capacity / mAh g^{-1}	Capacity after 100 cycles / mAh g^{-1}
$Li_4Ti_5O_{12}$	201	173
$Li_4Ti_{4.95}Zn_{0.05}O_{12}$	223	183
$Li_4Ti_{4.9}Zn_{0.1}O_{12}$	214	186
$Li_4Ti_{4.85}Zn_{0.15}O_{12}$	204	186
$Li_4Ti_{4.8}Zn_{0.2}O_{12}$	223	198

5 C charge-discharge rate	Initial capacity / mAh g^{-1}	Capacity after 200 cycles / mAh g^{-1}
$Li_4Ti_5O_{12}$	181	146
$Li_4Ti_{4.95}Zn_{0.05}O_{12}$	182	148
$Li_4Ti_{4.9}Zn_{0.1}O_{12}$	200	172
$Li_4Ti_{4.85}Zn_{0.15}O_{12}$	193	160
$Li_4Ti_{4.8}Zn_{0.2}O_{12}$	206	186

Fig. 7. Cycling performance of the $Li_4Ti_{5-x}Zn_xO_{12}$ samples at different charge–discharge rates. (a) 0.5 C, (b) 3 C and (c) 5 C.

in the diffraction peaks to the higher 2θ values for the sample Zn-doped LTO compared to pure LTO, indicating that the lattice parameter of the Zn-doped LTO samples is slightly smaller than that for the pure LTO samples. It may be explained by the following fact: (1) Zn^{2+} ion (0.74 Å [20]) has a smaller ionic radius than that of Li^+ of the octahedral sites (0.76 Å [12]), and then the Li^+ of the octahedral sites may be substituted Zn^{2+}; (2) there is a transition from Ti^{3+} ion (0.67 Å [20]) to Ti^{4+} ion (0.605 Å [20]) due to the divalent zinc doping. There is no (220) peak in $Li_4Ti_{4.95}Zn_{0.05}O_{12}$ as shown in Fig. 2, and this also can prove that no Zn^{2+} is located at the 8a sites according to Ref. [21]. Hence, the structure of $Li_4Ti_{5-x}Zn_xO_{12}$ may be shown the cation distribution to be $[Li_3]_{8a}[Li_y]_c[Li_{1-y}Ti_{5-x}Zn_x]_{16d}[O_{12}]_{32e}$. The intensity ratio of $I(311)/I(111)$ and $I(400)/I(111)$ obviously increases with increasing of the Zn-doped amount, indicating that the increased amount of Li^+ located at the 8a and 16c sites due to the Zn doping. The changes in these peaks' intensity also assure us that Zn^{2+} has entered the crystal lattice.

$Li_4Ti_{5-x}Zn_xO_{12}$ ($x = 0$, 0.05, 0.1, 0.15, 0.2) samples were investigated by Raman spectroscopy as plotted in Fig. 3. As shown in Fig. 3, five vibration peaks were observed at 253, 346, 425, 674 and 744 cm^{-1}, respectively. The two higher frequency bands (674 and 744 cm^{-1}) are assigned to the vibrations of Ti–O bonds in TiO_6 octahedra. The middle frequency bands in the range of Raman shift 300–500 cm^{-1} can be assigned to the stretching vibrations of the Li–O bonds in LiO_4 and LiO_6 polyhedra, respectively [22]. The Zn doping cannot change vibration characteristic of LTO, and this also indicates that Zn doping cannot change the basic $Li_4Ti_5O_{12}$ structure.

The SEM of the as-prepared $Li_4Ti_{5-x}Zn_xO_{12}$ ($x = 0$, 0.05, 0.1) in Fig. 4 shows that the material is well crystallized with a particle size in the range of 1–2 μm. It can be found that the Zn^{2+} substitution to some extent reduces the particle size of LTO.

The specific capacities of various $Li_4Ti_{5-x}Zn_xO_{12}$ samples determined by charge–discharge curves at a constant current density of 0.5 C between the cut-off voltages of 2.5 and 0.0 V are shown in Fig. 5. From the figures, it can be seen similar type of charge–discharge profiles for the doped and undoped specimens, revealing that the doping cannot change the basic spinel structure.

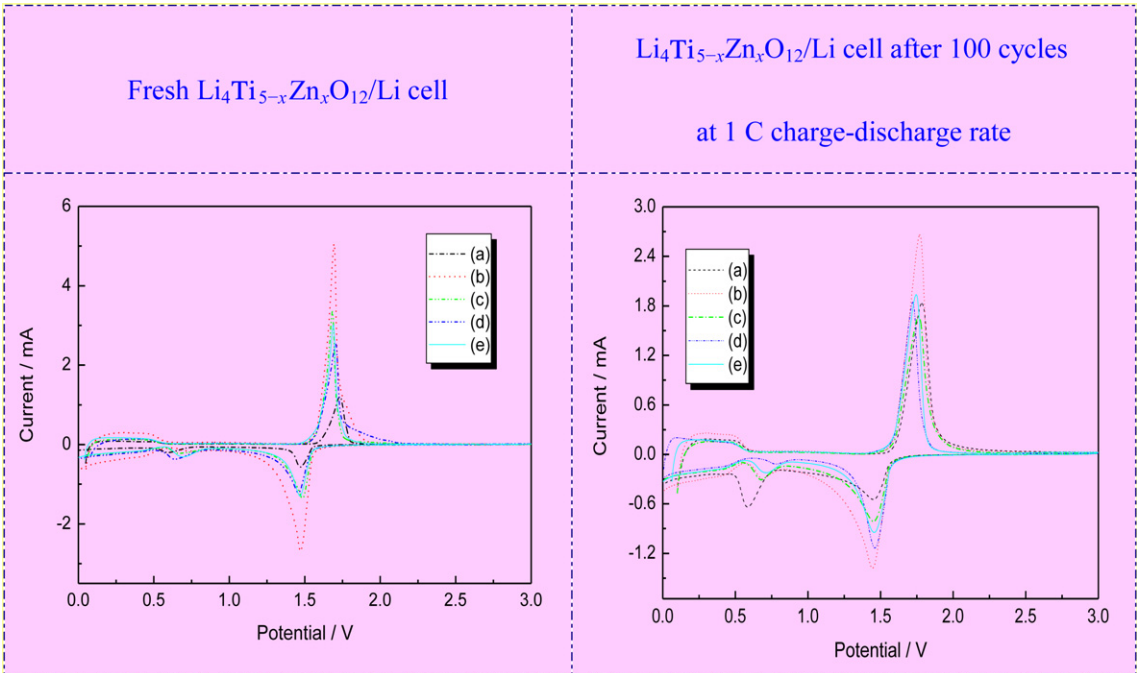

Sample	φ_a / V	φ_c / V	$(\varphi_a-\varphi_c)$ /m V	Sample	φ_a / V	φ_c / V	$(\varphi_a-\varphi_c)$ /m V
(a)	1.732	1.471	261	(a)	1.784	1.451	333
(b)	1.694	1.473	221	(b)	1.769	1.445	324
(c)	1.683	1.485	198	(c)	1.761	1.451	310
(d)	1.704	1.458	246	(d)	1.721	1.461	260
(e)	1.689	1.469	220	(e)	1.744	1.456	288

Fig. 8. Cyclic voltammetry (CV) and values of the CV peaks for $Li_4Ti_{5-x}Zn_xO_{12}$/Li cell between 0 V and 3 V: (a) $x = 0$, (b) $x = 0.05$, (c) $x = 0.1$, (d) $x = 0.15$ and (e) $x = 0.2$.

There are an obvious slope from 1.55 to 0.75 V, a plateau between 0.75 and 0.6 V, and an inclined curve from 0.6 to 0.0 V. It is obvious that zinc doping improves the initial discharge capacity of $Li_4Ti_5O_{12}$ charge–discharged at low rate (0.5 C), and the initial discharge capacity of $Li_4Ti_{4.8}Zn_{0.2}O_{12}$ arrives at 272 mAh g^{-1} that matches well with the expected theoretical capacity of 298 mAh g^{-1} for $Li_4Ti_5O_{12}$. In addition, Zn-doped LTO materials have a long discharge plateau at 1.55 V than that of pure LTO, indicting that Zn-doped LTO materials have a power density than that of pure LTO. The lower charge plateau of Zn-doped LTO than that of pure LTO shows that the charge acceptance of LTO doped by zinc may be better than the undoped LTO. The insertion/deinsertion of lithium in $Li_4Ti_5O_{12}$, $Li_7Ti_5O_{12}$ and $Li_9Ti_5O_{12}$ phases during charge–discharge processes is depicted schematically in Fig. 6. According to Fig. 6, $Li_{4+x}Ti_5O_{12}$ ($0 \le x \le 5$) can be further denoted as $[Li_3]_{8a}[\ ]_{16c}[Ti_5Li]_{16d}[O_{12}]_{32e}$ ($Li_4Ti_5O_{12}$), $[\ ]_{8a}[Li_6]_{16c}[Ti_5Li]_{16d}[O_{12}]_{32e}$ ($Li_7Ti_5O_{12}$) corresponding to the 1.55 V plateau and $[Li_x]_{8a}[Li_y]_{8b}[Li_6]_{16c}[Li_{2-x-y}]_{48f}[Ti_5Li]_{16d}[O_{12}]_{32e}$ ($Li_9Ti_5O_{12}$) corresponding to the capacity below 1.0 V. It is easy to understand all the electrochemical energy comes from reversible redox reactions between Ti^{3+} and Ti^{4+}.

Fig. 7 shows the cyclic performance of the $Li_4Ti_{5-x}Zn_xO_{12}$ ($x = 0$, 0.05, 0.1, 0.15, 0.2) samples at different charge–discharge rates. It can be observed that the Zn-doped samples exhibit high discharge capacity and good cycling stability at 3 C and 5 C rates. The capacity of $Li_4Ti_5O_{12}$ discharged at 3 C rate was 201 mAh g^{-1}, which was lower than the corresponding value of 223, 214, 204, and 223 mAh g^{-1} for $Li_4Ti_{5-x}Zn_xO_{12}$ ($x = 0$, 0.05, 0.1, 0.15, 0.2), respectively. After 100 cycles, $Li_4Ti_{5-x}Zn_xO_{12}$ ($x = 0.05$, 0.1, 0.15, 0.2) materials also have higher capacity than that of $Li_4Ti_5O_{12}$. As the discharge rate increased, the capacities gradually decreased. Under the high C rate, the doping effect on the rate capability becomes more pronounced. $Li_4Ti_{5-x}Zn_xO_{12}$ ($x = 0$, 0.05, 0.1, 0.15, 0.2) materials have higher initial capacity than that of $Li_4Ti_5O_{12}$ at 5 C rate, and Zn-doped materials have higher cycling performance than that of $Li_4Ti_5O_{12}$ at any rate mentioned above. It could be concluded that the high doping level is beneficial to enhance the electrochemical performance, especially when a high C rate charge/discharge is implemented. Fig. 7 clearly indicates excellent cyclic performance of $Li_4Ti_{4.8}Zn_{0.2}O_{12}$, with the doped other Zn-doped LTO powder having much better rate capability than the pure $Li_4Ti_5O_{12}$ powder. This shows that the Zn doping improves the rate capability of LTO, and the excellent rate capability may be attributed to the high electrical conductivity and fast lithium-ion diffusion. These excellent electrochemical properties make Zn-doped LTO a prime candidate for use as anode material in commercial lithium-ion batteries.

Fig. 8 presents typical cyclic voltammetry (CV) of $Li_4Ti_{5-x}Zn_xO_{12}$ ($x = 0$, 0.05, 0.1, 0.15, 0.2) materials after 0 and 100 cycles charge–discharged at 1 C rate. Both pristine $Li_4Ti_5O_{12}$ and Zn-doped LTO show a pair of sharp and reversible redox peaks at about 1.5 V, indicating the good electrode kinetic of all anodes. The cathodic peak (φ_c) located at around 1.5 V (versus Li^+/Li) corresponds to the voltage plateau of the first cycle discharge process in terms of which Li intercalated into the spinel $Li_4Ti_5O_{12}$ [23]. An anodic peak (φ_a) occurred at around 1.7 V versus Li^+/Li, corresponding to the flat voltage of charge process [24]. The potential difference ($\varphi_a - \varphi_c$) between anodic and cathodic peaks can reflect the polarization degree of the electrode [25,26]. For the fresh $Li_4Ti_{5-x}Zn_xO_{12}$/Li cell, the potential difference ($\varphi_a - \varphi_c$) of all Zn-doped LTO electrodes is lower than that of pure $Li_4Ti_5O_{12}$. After 100 cycles charge-discharged at 1 C, the potential difference ($\varphi_a - \varphi_c$) of all Zn-doped LTO electrodes is obviously lower than that of pure $Li_4Ti_5O_{12}$. This demonstrates that lithium ions are intercalation and deintercalation reversible in the Zn-doped LTO electrode.

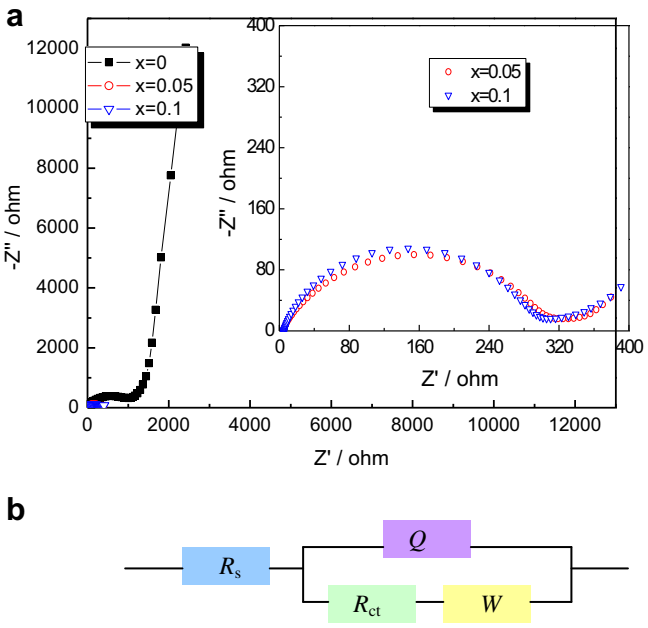

Fig. 9. (a) Nyquist plots and (b) equivalent circuit of $Li_4Ti_{5-x}Zn_xO_{12}$ ($x = 0$, 0.05, 0.1) electrode. Inset is the enlarged Nyquist plot of $Li_4Ti_{5-x}Zn_xO_{12}$ ($x = 0.05$, 0.1).

This observation suggests that the Zn doping enhances the reversibility of the LTO. These results are in agreement with the charge–discharge analysis given earlier.

To investigate the lithium-ion insertion mechanism at the electrode/electrolyte interface, EIS measurements were carried out for the fresh $Li_4Ti_{5-x}Zn_xO_{12}$ ($x = 0$, 0.05, 0.1) electrode. Fig. 9a shows the Nyquist plots obtained from the spinel $Li_4Ti_{5-x}Zn_xO_{12}$ ($x = 0$, 0.05, 0.1) electrode. Inset shows Nyquist plots for bulk $Li_4Ti_{5-x}Zn_xO_{12}$ ($x = 0.05$, 0.1). To understand this phenomenon better, the experimental impedance data was fitted to an equivalent circuit as plotted in Fig. 9b. In the EIS patterns, one semi-circle (high frequency region) and a straight line (low-frequency region) shapes are noted, which are related with the formation of SEI and diffusion of Li^+ ions [27,28]. In this equivalent circuit, W is the Warburg impedance of solid-phase diffusion [29], and R_s and R_{ct} represent the ohmic resistance and the charge transfer reaction related to lithium-ion interfacial transfer, coupled with a capacitance at the surface film/$Li_4Ti_5O_{12}$ particle interface [4]. The interfacial capacitance is represented by the constant phase elements (CPEs). The low-frequency region cannot be modeled properly by a finite Warburg element. We have chosen, therefore, to replace the finite diffusion by a CPE, i.e., Q. CPE involves double layer capacitance with a rough electrode surface, in the Nyquist plot, and it is shown with a characteristic of depressed semi-circle at high frequency region [30]. It can be seen from Table 1 that the R_s values of different samples are almost constant, whereas R_{ct} values vary greatly with different samples. The difference of R_s values between LTO and Zn-doped LTO may be caused by the simulated errors. Zn-doped LTO materials exhibit much lower charge transfer resistance than the pristine $Li_4Ti_5O_{12}$, and it may be explained by the following fact: (1) Zn doping can decrease the particle size

Table 1
Fitted results from EIS.

	$Li_4Ti_5O_{12}$	$Li_4Ti_{4.95}Zn_{0.05}O_{12}$	$Li_4Ti_{4.9}Zn_{0.1}O_{12}$
R_S/Ω	8.38	8.468	8.352
R_{ct}/Ω	663.4	289.2	283
$D_{Li}/cm^2\ s^{-1}$	7.48×10^{-15}	3.36×10^{-12}	1.38×10^{-12}

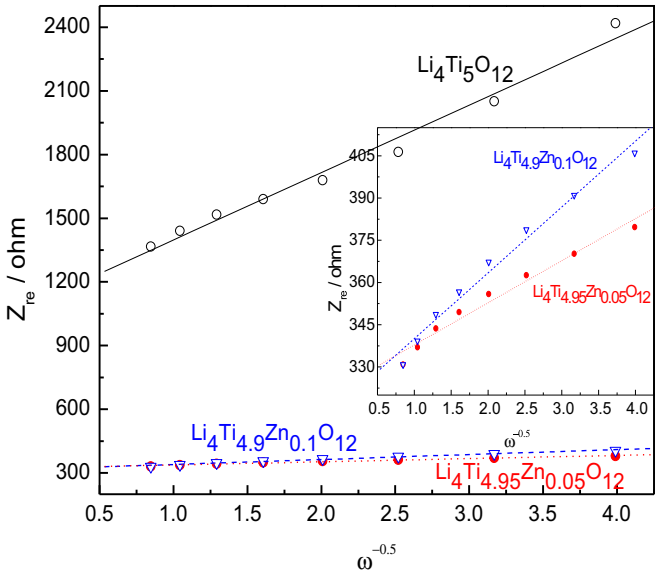

Fig. 10. Graph of Z_{re} plotted against $\omega^{-1/2}$ at low-frequency region for $Li_4Ti_{5-x}Zn_xO_{12}$ ($x = 0$, 0.05, 0.1) electrodes.

(Fig. 4) and thus increase the area for electrode reaction and shorten the diffusion path of the lithium ion; this factor can facilitate the charge transfer process and decreases the value of R_{ct}; (2) Zn doping improves the conductivity of LTO. As analyzed above, it is reasonable that the minimum R_{ct} value of Zn-doped LTO means a lower electrochemical polarization, and then leads to higher cycle performance at high charge–discharge rate.

The diffusion coefficient (D_{Li}) of lithium ion can be calculated from the plots in the low-frequency region. The equation for the calculation of D_{Li} values by EIS can be expressed as [31–33]:

$$Z_{re} = R_{ct} + R_s + \sigma\omega^{-\frac{1}{2}} \quad (1)$$

$$D_{Li} = \frac{(RT)^2}{2\left(An^2F^2C_{Li}\sigma\right)^2} \quad (2)$$

where the meanings of T is the absolute temperature, R the gas constant, n the number of electrons per molecule during oxidization, A the surface area, F the Faraday's constant, C_{Li} the concentration of lithium ion, ω the angular frequency, and σ is the Warburg factor which has relationship with Z_{re}. The Z_{re}–$\omega^{-1/2}$ plots are presented in Fig. 10. A linear characteristic could be seen for every curve. The diffusion coefficient of lithium ion is calculated based on Eqs. (1) and (2), and the calculated diffusion coefficients are given in Table 1. $Li_4Ti_{4.9}Zn_{0.1}O_{12}$ had a diffusion coefficient of 1.38×10^{-12} cm^2 s^{-1}, which is almost 185 times higher than 7.48×10^{-15} cm^2 s^{-1} for $Li_4Ti_5O_{12}$. This result clearly indicates that the lithium-ion mobility of $Li_4Ti_5O_{12}$ can be effectively improved by Zn doping. Based on the above results and discussion, divalent Zn^{2+} doping results in lower electrode polarization and a higher lithium-ion diffusion coefficient. Therefore, Zn doping can effectively improve the electrochemical performance of $Li_4Ti_5O_{12}$ in terms of discharge capacity, rate capability, etc.

4. Conclusion

$Li_4Ti_{5-x}Zn_xO_{12}$ ($x = 0$, 0.05, 0.15, 0.2) spinel was prepared by a solid-state reaction. The electrochemical reaction process has not been changed by Zn doping, as indicated by charge–discharge test and CV. Even though the material has a particle size of 1–2 μm, Zn-doped LTO shows very high rate capability and excellent capacity retention. The capacity of $Li_4Ti_{4.8}Zn_{0.2}O_{12}$ is as high as 186 mAh g^{-1} at a 5 C charge–discharge rate after 200 cycles. This high discharge rate performance of Zn-doped LTO is consistent with diffusion coefficient (D_{Li}) of lithium ion of the activation barrier for lithium motion. $Li_4Ti_{4.9}Zn_{0.1}O_{12}$ had a diffusion coefficient of 1.38×10^{-12} cm^2 s^{-1}, which is almost 185 times higher than 7.48×10^{-15} cm^2 s^{-1} for $Li_4Ti_5O_{12}$. This observation suggests that the Zn doping enhances the reversibility of the LTO. The ease of synthetic preparation of Zn-doped LTO anode material together with its stable electrochemical performance at high charge–discharge rate shows promise for high-power energy storage applications.

Acknowledgments

This work was financially supported by the National Natural Science Foundation of China (no. 50902001), the Key project of Scientific Research Foundation sponsored by Education Department of Anhui Province, China (no. KJ2010A045), and the Foundation for Young Talents in College of Anhui Province, China (no. 2010SQRL033ZD). The work is also supported by the Program for Innovative Research Team in Anhui University of Technology (no. TD201202).

References

[1] J. Hassoun, P. Reale, S. Panero, B. Scrosati, M. Wachtler, M. Fleischhammer, M. Kasper, M. Wohlfahrt-Mehrens, Electrochim. Acta 55 (2010) 4194–4200.
[2] S.S. Zhang, J. Power Sources 161 (2006) 1385.
[3] J. Lim, E. Choi, V. Mathew, D. Kim, D. Ahn, J. Gim, S.-H. Kang, J. Kim, J. Electrochem. Soc. 158 (2011) A275–A280.
[4] Y.G. Wang, H.M. Liu, K.X. Wang, H. Eiji, Y.R. Wang, H.S. Zhou, J. Mater. Chem. 19 (2009) 6789–6795.
[5] L. Chen, J. Yan, G.N. Zhu, J.Y. Luo, C.X. Wang, Y.Y. Xia, J. Mater. Chem. 19 (2010) 595–602.
[6] K. Amine, I. Belharouak, Z.H. Chen, T. Tran, H. Yumoto, N. Ota, S.T. Myung, Y.K. Sun, Adv. Mater. 22 (2010) 3052–3057.
[7] H.-G. Jung, S.-T. Myung, C.S. Yoon, S.-B. Son, K.H. Oh, K. Amine, B. Scrosati, Y.-K. Sun, Energy Environ. Sci. 4 (2011) 1345–1351.
[8] D. Ahn, X. Xiao, Electrochem. Commun. 13 (2011) 796–799.
[9] K.-S. Park, A. Benayad, D.-J. Kang, S.-G. Doo, J. Am. Chem. Soc. 130 (2008) 14930–14931.
[10] B. Zhang, H. Du, B. Li, F. Kang, Electrochem. Solid-State Lett. 13 (2010) A36–A38.
[11] B. Tian, H. Xiang, L. Zhang, Z. Li, H. Wang, Electrochim. Acta 55 (2010) 5453–5458.
[12] T.-F. Yi, Y. Xie, J. Shu, Z. Wang, C.-B. Yue, R.-S. Zhu, H.-B. Qiao, J. Electrochem. Soc. 158 (2011) A266–A274.
[13] T.-F. Yi, L.-J. Jiang, J. Shu, C.-B. Yue, R.-S. Zhu, H.-B. Qiao, J. Phys. Chem. Solids 71 (2010) 1236–1242.
[14] T.-F. Yi, J. Shu, Y.-R. Zhu, X.-D. Zhu, R.-S. Zhu, A.-N. Zhou, J. Power Sources 195 (2010) 285–288.
[15] M. Venkateswarlu, C.H. Chen, J.S. Do, C.W. Lin, T.C. Chou, B.J. Hwang, J. Power Sources 146 (2005) 204–208.
[16] Y. Bai, F. Wang, F. Wu, C. Wu, L.-y. Bao, Electrochim. Acta 54 (2008) 322–327.
[17] S.Y. Yin, L. Song, X.Y. Wang, M.F. Zhang, K.L. Zhang, Y.X. Zhang, Electrochim. Acta 54 (2009) 5629–5633.
[18] S. Zhang, P. Shi, Electrochim. Acta 49 (2004) 1475–1482.
[19] J.Y. Song, H.H. Lee, Y.Y. Wang, C.C. Wan, J. Power Sources 111 (2002) 255–267.
[20] R.D. Shannon, Acta Crystallogr. A32 (1976) 751–767.
[21] C.H. Chen, J.T. Vaughey, A.N. Jansen, D.W. Dees, A.J. Kahaian, T. Goacher, M.M. Thackeray, J. Electrochem. Soc. 148 (2001) A102–A104.
[22] R. Baddour-Hadjean, J.-P. Pereira-Ramos, Chem. Rev. 110 (2010) 1278.
[23] L. Kavan, J. Procházka, T.M. Spitler, M. Kalbáč, M. Zukalová, T. Drezen, M. Grätzel, J. Electrochem. Soc. 150 (2003) A1000.
[24] Y. Qi, Y. Huang, D. Jia, S.-J. Bao, Z.P. Guo, Electrochim. Acta 54 (2009) 4772.
[25] T. Yuan, X. Yu, R. Cai, Y. Zhou, Z. Shao, J. Power Sources 195 (2010) 4997–5004.
[26] T.-F. Yi, J. Shu, Y.-R. Zhu, X.-D. Zhu, C.-B. Yue, A.-N. Zhou, R.-S. Zhu, Electrochim. Acta 54 (2009) 7464–7470.
[27] Q.-C. Zhuang, T. Wei, L.-L. Du, Y.-L. Cui, L. Fang, S.-G. Sun, J. Phys. Chem. C 114 (2010) 8614–8621.

[28] D. Aurbach, K. Gamolsky, B. Markovsky, G. Salitra, Y. Gofer, U. Heider, R. Oesten, M. Schmidt, J. Electrochem. Soc. 147 (2000) 1322.
[29] G.T.-K. Fey, C.Z. Lu, T.P. Kumar, J. Power Sources 115 (2003) 332.
[30] L. Yang, L. Gao, J. Alloys Compd. 485 (2009) 93.
[31] A.Y. Shenouda, H.K. Liu, J. Power Sources 185 (2008) 1386.
[32] G.Q. Liu, H.T. Kuo, R.S. Liu, C.H. Shen, D.S. Shy, X.K. Xing, J.M. Chen, J. Alloys Compd. 496 (2010) 512.
[33] Q. Cao, H.P. Zhang, G.J. Wang, Q. Xia, Y.P. Wu, H.Q. Wu, Electrochem. Commun. 9 (2007) 1228.